DEVELOPMENT OF BEAM CURRENT MONITOR WITH HIGH-Tc SQUID AT RIBF

T. Watanabe*, N. Fukunishi, Y. Sasaki, M. Kase, A. Goto and O. Kamigaito
RIKEN Nishina Center for Accelerator-Based Science, Wako-shi, Saitama 351-0198, Japan

Abstract

A highly sensitive beam current monitor with a high-critical-temperature (high-Tc) superconducting quantum interference device (SQUID) and a high-Tc current sensor, that is, a high-Tc SQUID monitor, has been developed for use in the radioisotope beam factory (RIBF) at RIKEN. As reported in the present work, the high-Tc SQUID monitor allows us to measure the DC of high-energy heavy-ion beams nondestructively in such a way that the beams are diagnosed in real time and the beam current extracted from the cyclotron can be recorded without interrupting beam user experiments. Both the high-Tc magnetic shield and the high-Tc current sensor were fabricated by dip-coating a thin layer of Bi_2-Sr_2-Ca_2-Cu_3-O_x (2223-phase, Tc=106 K) on a 99.9% MgO ceramic substrate. Unlike other existing facilities, all the high-Tc devices are cooled by a low-vibration pulse-tube refrigerator, enabling us to downsize the system. Last year, aiming at its practical use, the high-Tc SQUID monitor was installed in the RIBF. Using the monitor, a 1 μA Xe beam intensity (50 MeV/u) was successfully measured with 100 nA resolution. Here we report the present status of the facility, details of the high-Tc SQUID monitoring system and the results of the beam measurement.

INTRODUCTION

Accelerator complex of RIBF

The RIBF project to accelerate all elements from hydrogen to uranium up to an energy of 440 MeV/u for light ions and 350 MeV/u for heavy ions started in April 1997 [1]. Figure 1 shows a schematic layout of the RIBF facility. The research activities in the RIBF project make extensive use of the heavy-ion accelerator complex, which consists of one linac and four ring cyclotrons, i.e., a variable-frequency linac (RILAC), the RIKEN ring cyclotron (RRC), a fixed-frequency ring cyclotron (fRC), an intermediate-stage ring cyclotron (IRC) and a superconducting ring cyclotron (SRC). Energetic heavy-ion beams are converted into intense RI beams via the projectile fragmentation of stable ions or the in-flight fission of uranium ions using a superconducting isotope separator, BigRIPS [2]. The combination of these accelerators and BigRIPS is expected to greatly expand our knowledge of the nuclear world into the presently inaccessible region on the nuclear chart. We succeeded in accelerating a uranium beam to 345 MeV/u in March 2007, by which new RIs, the neutron-rich palladium isotopes of $_{125}$Pd and $_{126}$Pd, were discovered [3, 4].

In 2008, the RIBF succeeded in providing heavy-ion beams of $_{48}$Ca and $_{238}$U with particle currents of 170 pnA and 0.4 pnA, respectively, at an energy of 345 MeV/u. The search for new isotopes using in-flight fission of the 345 MeV/u uranium beam has continued. Consequently, fission fragments have been analyzed and identified using BigRIPS and we have observed 45 new neutron-rich isotopes. From the operational point of view, however, the intensity of the uranium beam should be greatly increased. Furthermore, RIBF research conflicts with ongoing research on the synthesis of super-heavy elements using a gas-filled recoil separator (GARIS), because both of them use the RILAC. To reconcile this conflict, a new additional injector linac for the RIBF (RILAC2) has been proposed and is now under construction. We have therefore constructed a superconducting electron cyclotron resonance (ECR) ion source that is capable of providing a microwave power of 28 GHz, a radio frequency quadrupole (RFQ) linac and three drift tube linacs (DTLs). The new injector, which will be ready in FY2010, will hopefully enable the independent operation of the RIBF experiments and research on super-heavy element synthesis [5].

Technical issues related to Faraday cups

It is essential to keep the beam transmission efficiency as high as possible, because the production of the RI beam requires an intense primary beam during beam user experiments. Furthermore, activation produced by beam loss should be particularly avoided. In this facility, to evaluate the beam transmission efficiency, about 50 Faraday cups are used. A Faraday cup is used in the conventional method of measuring the beam current. However, the beam cannot be used while it is being measured, and there is a danger of melting and activating the cup. Furthermore, it is difficult to completely suppress the high-energy secondary electrons that are produced by heavy-ion beams. When an accelerated particle collides with the surface of a Faraday cup, secondary electrons are always generated. If these electrons escape from the insulated cup area, the reading of the beam current is incorrect by the number of lost electrons. Thus, the suppression of secondary electrons is very important for measuring the beam current precisely. Normally, this can be achieved by applying a high negative voltage close to the entrance of the cup. However, since the electrical field on the beam axis is lower

* wtamaki@riken.jp

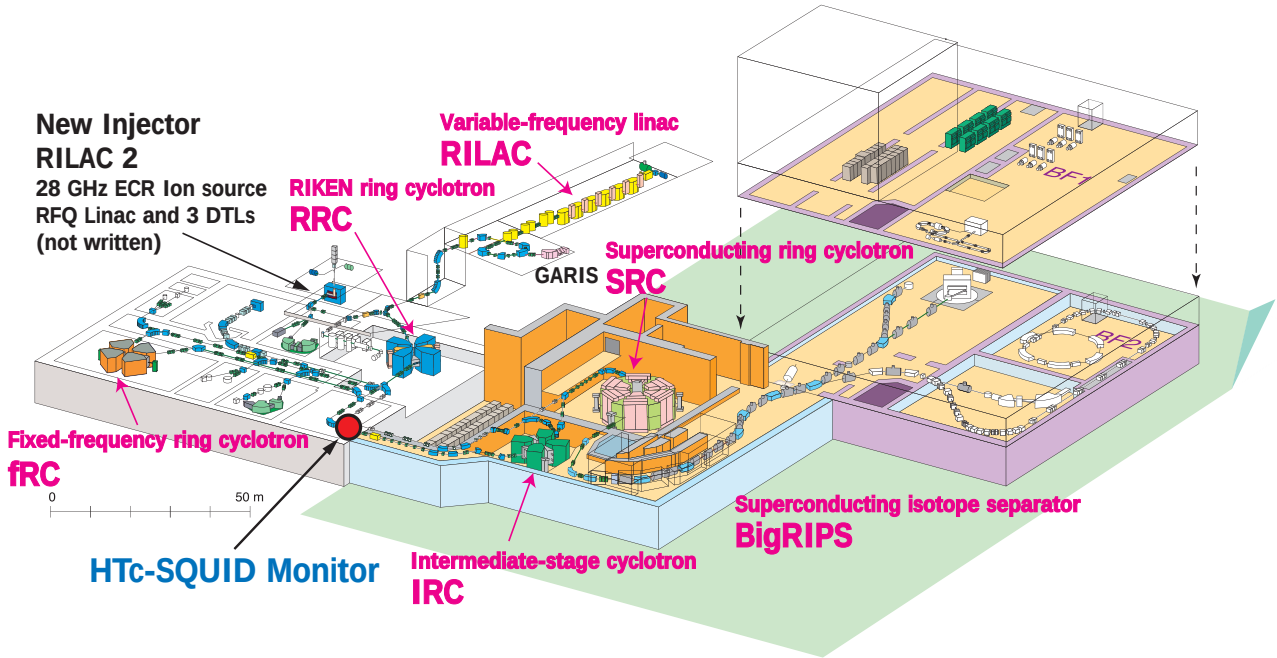

Figure 1: Schematic bird's-eye view of the RIBF facility.

than that on the edge, it is difficult to completely suppress the high-energy secondary electrons that are produced by high-energy heavy-ion beams. To evaluate the number of secondary electrons generated by a beam, a high positive voltage is used for suppression. A measurement result obtained by applying the suppression voltage for a 10.7 MeV/u $^{238}_{92}U^{72+}$ beam is shown in Fig. 2. From this result, the current generated by the secondary electrons was found to be eight times stronger than that of the uranium beam. To resolve this technical issue, a study of the high-Tc SQUID monitor has been started at RIKEN [6, 7, 8]. The high-Tc SQUID monitor has been installed in the beam transport line between the fRC and the IRC aiming at its practical use in the RIBF.

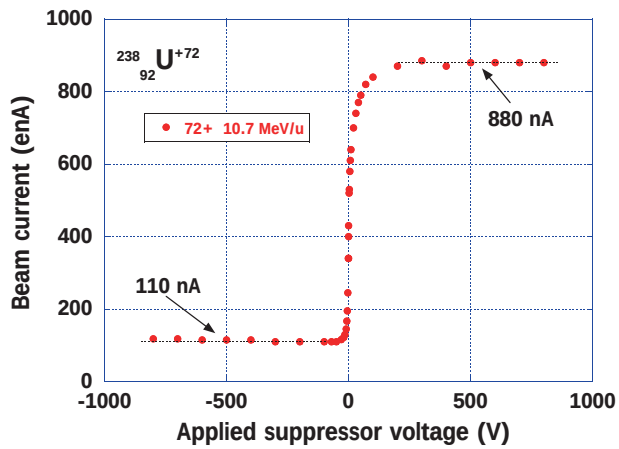

Figure 2: Measurement result obtained by applying suppression voltage for 10.7 MeV/u $^{238}_{92}U^{72+}$ beam. To evaluate the number of secondary electrons generated by the beam, a high positive voltage was used for suppression.

Cryogenic current comparator

The application of superconducting technology to the precise measurement of current has been extensively developed for the liquid helium regime [9]. The first cryogenic current comparator, the so-called CCC, based on SQUIDs for measuring beam currents was built at PTB in Berlin in 1977 [10]. This group was the first to use a CCC based on SQUIDs for measuring beam current, and a 108 nA electron beam generated by a Van de Graaff accelerator was observed. Because the accelerator at the PTB was shut down and it became difficult to fabricate the SQUID, the development of this device was stopped. However, modern technologies that apply superconductivity have led to a new era of accelerators. A new type of CCC has been built at GSI, and a 300 MeV/u neon beam extracted from SIS, the heavy-ion synchrotron at GSI, was measured [11]. In 2001, the group of Dr. L. Hao began investigating high-Tc CCC designs incorporating a flux concentrator and a high-Tc SQUID. They outlined a proposal for the precise determination of the Faraday fundamental constant using a purely physical system and employing a high-Tc CCC to measure the current of charged particle beams [12].

Motivation

In the present work, the reason for using the SQUID as a beam current monitor is that it has a very high magnetic

Table 1: Comparison of cooling costs.

	1 day	1 year
Liquid He for low-Tc	\$430 (20L / day)	\$157,000
Refrigerator for high-Tc	\$10 (1.9kW / day)	\$3,650

sensitivity. The Earth's magnetic field is on the order of 10^{-5} T and that of environmental noise is on the order of 10^{-6} T. On the other hand, the range of the magnetic field induced by the heart and brain and measured by SQUIDs is from 10^{-10} to 10^{-13} T. Furthermore, the magnetic field produced by a 1 nA beam at a distance of 10 cm is 2×10^{-15} T, ten orders of magnitude smaller than the Earth's magnetic field. From this comparison, it becomes apparent how difficult it is to measure the current of a faint beam. The sensitivity of a DC current transformer (DCCT) is about 1 μA. The function of a DCCT is based on the modulation of a magnetic material, and the limiting factor is the Barkhausen noise produced by the wall-jumping of a magnetic region. In the present work, by using high-Tc devices including the SQUID, we aim to downsize the system and reduce the running costs. This is illustrated by comparing the costs of a low-Tc SQUID monitor and a high-Tc SQUID monitor, which have operational temperatures of the superconductor and the SQUID of 4.2 K and 77.3 K, respectively. If the low-Tc SQUID monitor consumes 20 L of liquid helium per day [13], it costs a total of \$157,000 per year. On the other hand, the high-Tc SQUID monitor only requires electricity, costing about \$3,650 per year. Table 1 shows a comparison of the cooling costs, which were estimated using Japanese prices. Its low cost is the major advantage of using the high-Tc SQUID monitor.

HIGH-T_C SQUID MONITORING SYSTEM

Fundamental principles of high-Tc SQUID monitor

A schematic drawing of the high-Tc SQUID monitoring system is shown in Fig. 3(a). Both the high-Tc magnetic shield and the high-Tc current sensor were fabricated by dip-coating a thin Bi_2-Sr_2-Ca_2-Cu_3-O_x (Bi-2223) layer on a 99.9% MgO ceramic substrate. When a charged particle (ion or electron) beam passes along the axis of the high-Tc tube, a shielding current produced by the Meissner effect flows in the opposite direction along the wall of the high-Tc tube so as to screen the magnetic field generated by the beam. Since the outer surface is designed to have a bridge circuit (Fig. 3(b)), the current generated by the charged particle beam is concentrated in the bridge circuit and forms an azimuthal magnetic field Φ around the bridge circuit. The high-Tc SQUID is set close to the bridge circuit and can detect the azimuthal magnetic field with a high S/N ratio. In particular, we adopt a SQUID gradiometer to increase the S/N ratio (Fig. 6). Since the SQUID gradiometer has two pickup coils that are wound in opposite directions and

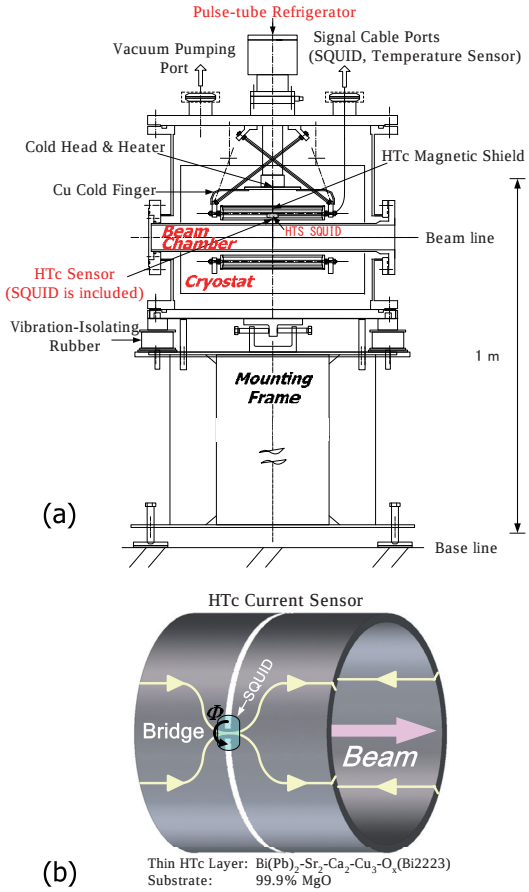

Figure 3: Schematic drawing of the high-Tc SQUID monitoring system (a) and the current sensor (b).

connected in series, the signal level is expected to be improved by a factor of 2, while the background noise can be significantly reduced by more than 40 dB.

The high-Tc SQUID monitoring system consists of two vacuum chambers completely separate from each other:

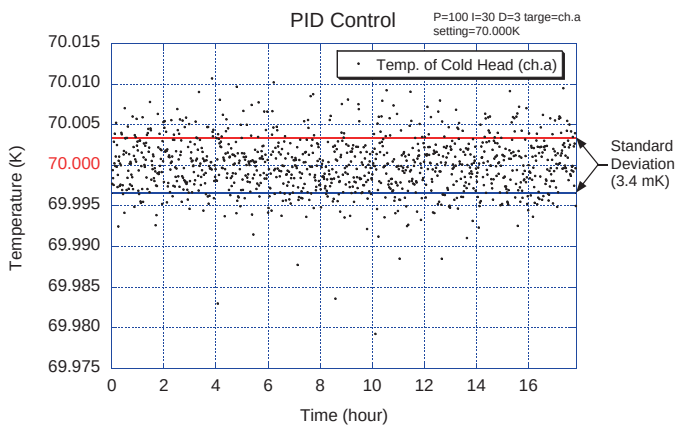

Figure 4: Plots of the temperature of the cold head as a function of time. The standard deviation of the temperature over a period of 18 h was 3.4 mK.

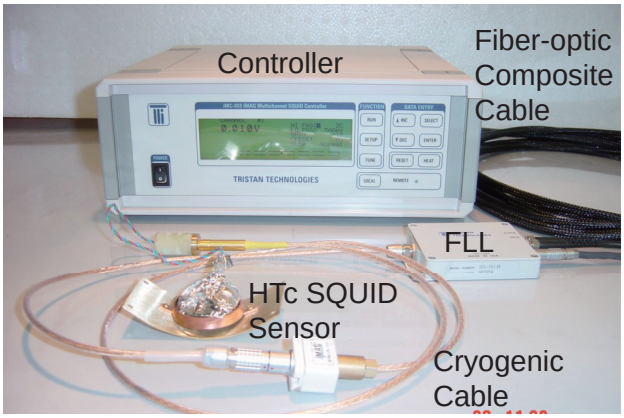

Figure 5: High-Tc SQUID system (Model BMS-G, manufactured by Tristan Technologies) [14].

one chamber contains a cryostat in which the high-Tc SQUID, a high-Tc magnetic shield and a high-Tc current sensor are cooled, and the beam passes through the other chamber. In the present work, all the fabricated high-Tc devices are cooled by a low-vibration pulse-tube refrigerator with a refrigeration power of 11 W at a temperature of 77 K. The operation temperature can be adjusted in the range of 64 K to 90 K (the critical temperature of the high-Tc SQUID) using a heater, since the pulse-tube refrigerator is capable of cooling the system to temperatures lower than liquid-nitrogen temperature. Furthermore, it is possible to stabilize the temperature of the high-Tc SQUID with an accuracy of 5 mK using a PID feedback controller, which includes four thermometers and a heater. PID stands for proportional, integral and derivative and the PID feedback controller calculates these three separate parameters. The temperature of the cold head was measured as a function of time. Figure 4 shows plots of the temperature of the cold head as a function of time. The deviation of the temperature over a period of 18 h was controlled within 3.4 mK (1σ) . The high-Tc SQUID system (Model BMS-G, manufactured by Tristan Technologies [14]) contains an HTG-10R low-noise high-Tc SQUID gradiometer (Y-Ba_2-$Cu_3O_{7-\delta}$) [15, 16, 17], a controller, a flux-locked loop (FLL), a cryogenic cable and a fiber-optic composite cable. Figure 5 shows the high-Tc SQUID system, and the specifications

Table 2: Specifications of the high-Tc DC SQUID system.

Noise level	34 fT/cm/$\sqrt{Hz}$ @ 5 kHz
Operation temperature	77 K
Feedback gain	1, 2 ,5, 10, 20, 50, 100, 200, 500
High-pass filter	DC, 0.3 Hz
Low-pass filter	5 Hz, 500 Hz, 5 kHz, 25 kHz
Data accuracy (AD)	16 bit
Data acquisition rate	20,000 words/s
Remote control	IEEE-488, RS-232

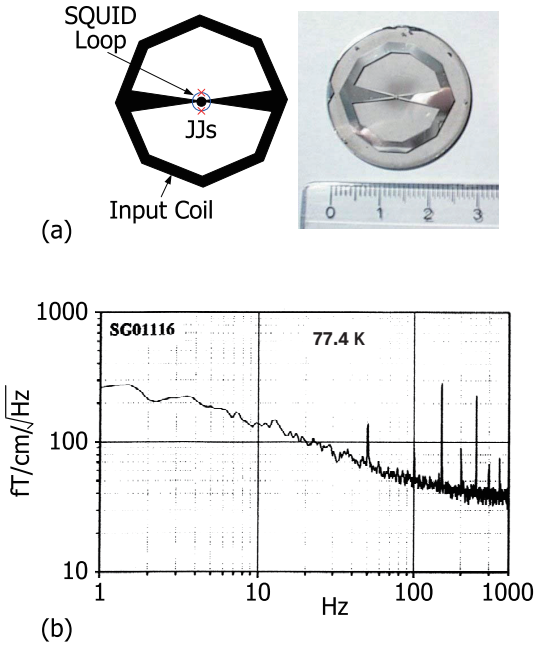

Figure 6: (a) Schematic drawing and photograph of the high-Tc SQUID gradiometer (HTG-10R [15, 16, 17]). (b) Measured noise spectrum in frequency domain, indicating a 1/f noise structure. White noise is reasonably low compared with the case of using a conventional high-Tc SQUID, in which white noise is over 1 pT/cm/$\sqrt{Hz}$.

of the system are given in Table 2. The high-Tc SQUID gradiometer is composed of an input coil and a SQUID loop with two Josephson junctions (Fig. 6(a)). Figure 6(b) shows the measured noise spectrum in the frequency domain, which indicates a 1/f noise structure. White noise is reasonably low compared with the case of using a conventional high-Tc SQUID, in which white noise is over 1 pT/cm/$\sqrt{Hz}$. The coefficient of the magnetic field relative to the output voltage of the SQUID gradiometer is 2.43 nT/V when the maximum gain of 500 is selected.

Principle of SQUID operation

A DC SQUID consists of two superconductors separated by thin insulating layers to form two parallel Josephson junctions (Fig. 7). A constant bias current I_b is maintained at the critical current, which is the maximum current that a superconductor can carry with zero resistance. The critical current changes periodically in response to a magnetic flux quantum phi zero of 2.07×10^{-15} weber. Therefore, this results in the voltage also changing similarly to the absolute value of the cosine function in response to the magnetic flux quantum.

The SQUID sensor is typically operated in a null detection mode where the FLL provides a negative feedback to maintain a linear operation as shown in Fig. 8. The modulated SQUID signal is amplified, filtered, demodulated and integrated in the FLL. Thus, the FLL output signal is pro-

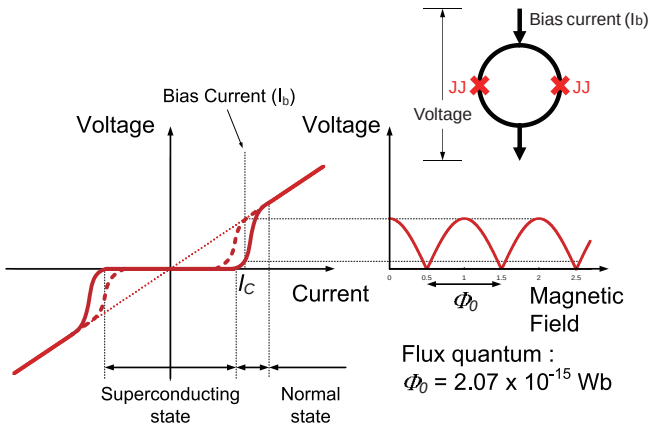

Figure 7: Principle of SQUID operation.

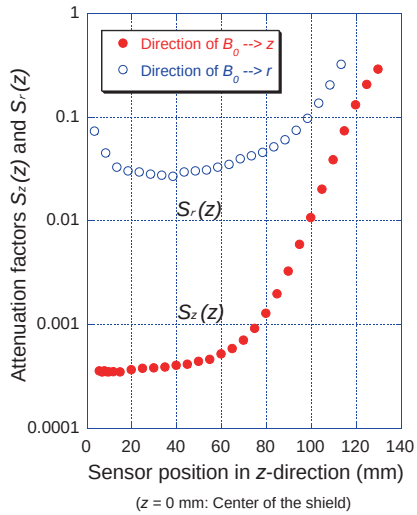

Figure 9: Measurement results for attenuation factors $S_z(z)$ and $S_r(z)$, where the directions of the external magnetic field B_0 (3.5 μT, 1 Hz) are the z-direction (•) and x-direction (○), respectively.

portional to the change in magnetic flux density B at the SQUID pickup coil. A modulation oscillator and a synchronous detector are used to create an FLL circuit similar to a negative feedback phase-locked circuit. The sensor package (shaded region) in Fig. 8 is kept below the critical temperature T_c.

High-Tc and permalloy shields

A cylindrical Bi-2223 high-Tc magnetic shield (148 mm diameter and 250 mm length) was fabricated by dip-coating a thin (300 μm) Bi-2223 layer on a 99.9% MgO ceramic substrate. A high-Tc magnetic shield has an advantage that the magnetic shielding effect is independent of the frequency of environmental magnetic noise, even in the low-frequency band [20]. The critical current (I_c) of 4500 A/cm^2 and the critical temperature (T_c) of 106 K of the Bi-2223 cylindrical high-Tc shield were obtained by a DC four-probe method using a small sample of Bi-2223. To measure the field distribution inside the high-Tc shield and to obtain the attenuation factors, we constructed a measurement system [19]. The system is composed of an X-Y-Z stage driven by stepping motors, a G10 rod which is fixed on the X-Y-Z stage and attached to two high-Tc SQUID probes, a liquid N_2 Dewar vessel and a Helmholtz coil that supplies an external field. Hereafter, we define the direction of the cylindrical axis as the z-direction and the direction perpendicular to the axis as the r-direction. If the external fields B_{z0} and B_{r0} exist, the attenuation factors

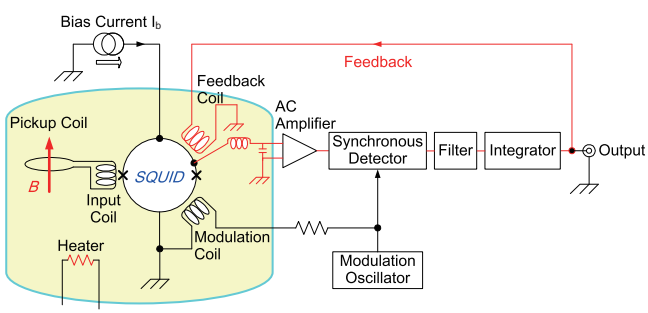

Figure 8: The SQUID sensor is typically operated in a null detection mode where the FLL provides a negative feedback to maintain a linear operation. The modulated SQUID signal is amplified, filtered, demodulated and integrated in the FLL. Thus, the FLL output signal is proportional to the change in magnetic flux density B at the SQUID pickup coil. The sensor package (shaded region) is kept below the critical temperature T_c.

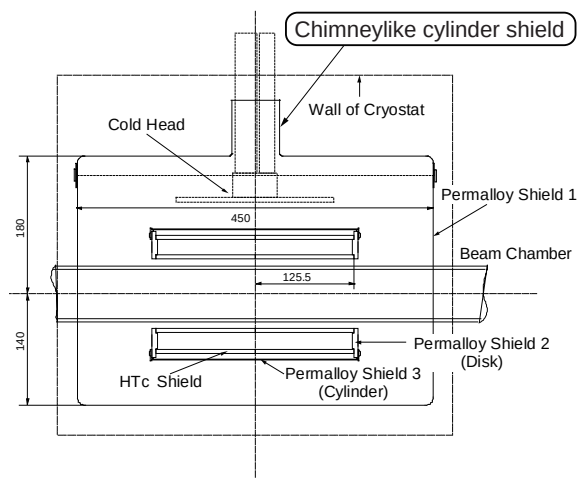

Figure 10: Magnetic shields composed of high-Tc shield, permalloy shield 1, permalloy shield 2 (disk) and permalloy shield 3 (cylinder).

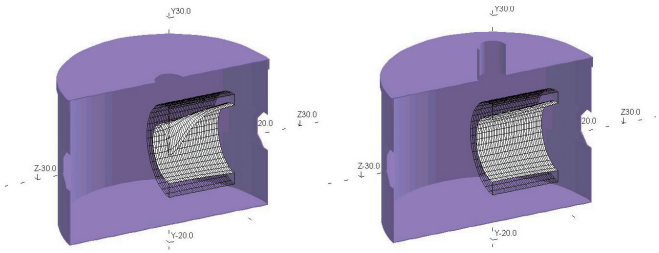

Figure 11: Calculated results showing that the shielding effect is improved when a chimney-like cylinder shield is added.

$S_z(z)$ and $S_r(z)$ are defined as

$$S_z(z) = B_z(z)/B_{z0},$$
$$S_r(z) = B_r(z)/B_{r0},$$

where $B_z(z)$ and $B_r(z)$ are the z and r components of the magnetic field at position z, respectively. Figure 9 shows the measurement results for attenuation factors $S_z(z)$ and $S_r(z)$, where the directions of the external magnetic field B_0 (3.5 μT, 1 Hz) are the z-direction (•) and x-direction (○), respectively. From these measurement results, the attenuation factors of $S_z(0) = 5 \times 10^{-4}$ and $S_r(0) = 8 \times 10^{-2}$ were obtained.

Because the attenuation factor of $S_r(0)$ of the high-Tc magnetic shield is too large, we attempt to reinforce the high-Tc magnetic shield. On the basis of various calculations using the finite element method program OPERA-3d [20], three permalloy shields, permalloy shield 1, permalloy shield 2 (disk) and permalloy shield 3 (cylinder), were constructed around the high-Tc shield, as shown in Fig. 10. A calculation showed that the shielding effect with a chimneylike cylinder shield is three times higher than that without the shield (see Fig. 11). To confirm the shielding effect of the reinforced system, a measurement was carried out. A field of 10^{-5} T produced by a Helmholtz coil was attenuated to 10^{-11} T, which was measured by the SQUID. A strong magnetic shielding system having an attenuation factor of 10^{-6} was thus obtained.

Beam position

We investigated whether the principle of a conventional beam position monitor could be applied to the SQUID monitor. The beam position pickup has a pair of isolated electrodes (or two pairs if two beam position coordinates are being measured). The deviation of the beam center with respect to the vacuum chamber can be monitored by measuring the difference in the voltage of each electrode induced by the beam.

We then fabricated a smaller version of the position sensor, as shown in Fig. 12(a). The high-Tc current sensor is divided into two parts by a slit, and a high-Tc SQUID is set on each bridge. To measure the position dependence

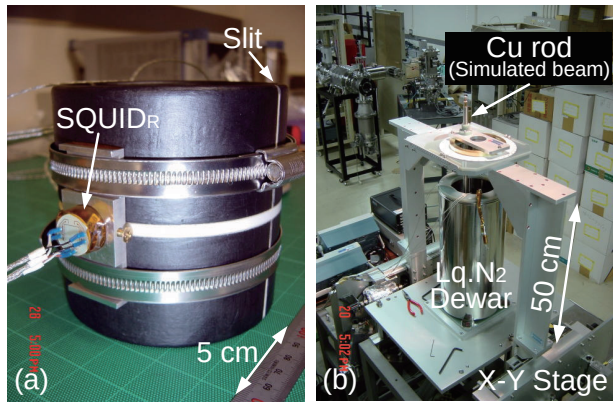

Figure 12: (a) Smaller version of position sensor, which is divided into two parts by a slit; a SQUID is set on each bridge. (b) Position measurement system, which is composed of an X-Y stage driven by stepping motors and a Cu rod, which is fixed on the X-Y stage and plays the role of a simulated beam.

of the output voltage of each SQUID, we converted a measurement system that had been used to measure the field distribution inside a high-Tc magnetic shield into a position measurement system. This system is composed of an X-Y stage driven by stepping motors and a Cu rod, which is fixed on the X-Y stage and simulates a beam. Figure 13 shows a schematic drawing of the position sensor, where D is the width of the sensor, Δx is the beam position from the center, and V_R and V_L represent the output voltage of each SQUID. If the beam is positioned at the center, the output of each SQUID should be equal. However, if the beam is shifted to the right side, it is expected that the output voltage V_R will be larger than V_L. Usually, the beam position

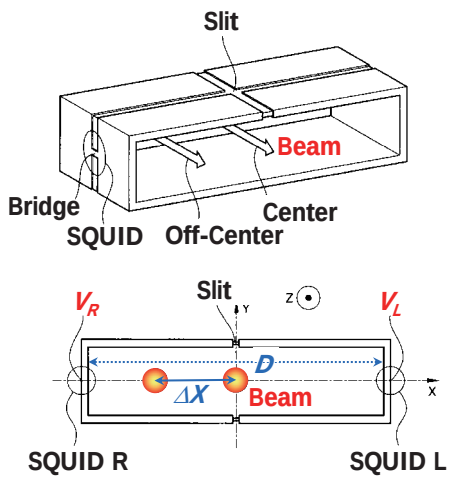

Figure 13: Schematic drawing of the current sensor of the high-Tc SQUID monitor.

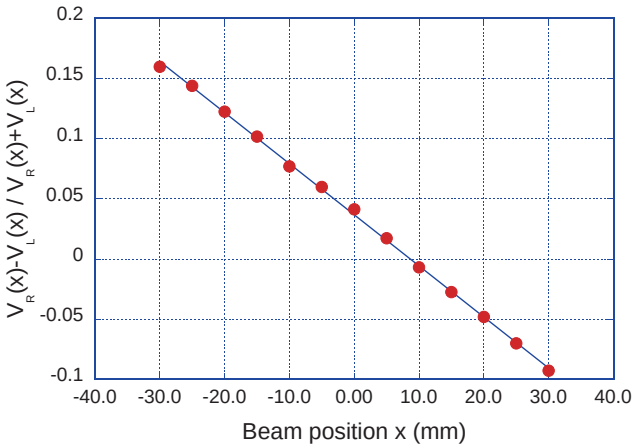

Figure 14: Measured values of Δ/Σ plotted versus the Cu rod position when a sinusoidal simulated current (1 mA, 5 Hz) was used.

Δx is obtained by the following relationship:

$$\Delta x = \frac{1}{\varepsilon}\frac{D}{2}\frac{\Delta}{\Sigma} = \frac{1}{\varepsilon}\frac{D}{2}\frac{V_R - V_L}{V_R + V_L},$$

where ε is the position sensitivity of the monitor. The measured values of Δ/Σ are plotted versus the Cu rod position in Fig. 14, for which a sinusoidal simulated current (1 mA, 5 Hz) was used, and thus we discovered that the beam position and beam current can be measured simultaneously in real time by dividing the current sensor into two parts and setting a SQUID on each bridge. The output voltage of the right SQUID, V_R, is not equal to that of the left SQUID, V_L, when the simulated beam is positioned at the center according to Fig. 14 because the output voltage of the SQUID is very sensitive to the setting accuracy. However, it was difficult to install the SQUIDs on the bridge accurately because each SQUID was bound by two stainless-steel bands (Fig. 12).

EXPERIMENTAL RESULTS

Prior to the beam measurements in the RRC hall, preliminary measurements were successfully carried out as follows: (1) a first beam test of the high-Tc SQUID monitoring system in the beam transport line of the ECR ion source in the CNS experimental hall and (2) a second beam measurement at the E1 experimental hall in RIKEN to measure the current of the high-energy heavy-ion beam. Aiming at its practical use for accelerator operations, the authors installed the high-Tc SQUID monitoring system in the beam transport line in the RRC hall (Fig. 1).

However, the SQUID electric circuit, which has a dynamic range of 100 dB (from 1 μA to 0.1 A) and a frequency range from DC to 25 kHz, did not function normally owing to the following reasons: (1) an RF background was caused by the high-power RF cavities of the RRC, which can produce a total power of 0.6 MW; (2) a

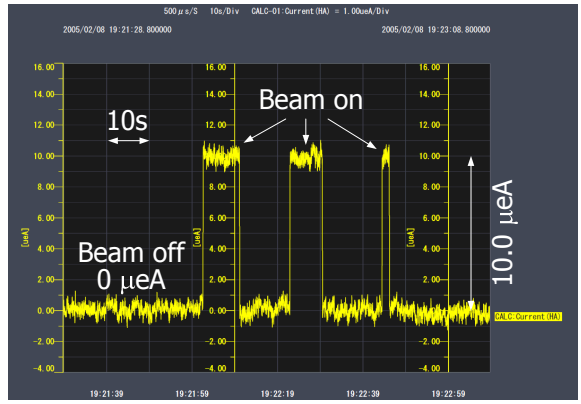

Figure 15: A 10 μA $^{40}Ar^{15+}$ beam intensity (63 MeV/u) was succesfully measured in real time with 500 nA resolution when a 1 μA beam produced a magnetic flux of $6.5\times10^{-3}\Phi_0$ at the input coil of the high-Tc SQUID.

large stray magnetic field was induced by the main magnetic field of the RRC (max. 1.67 T); (3) there was a neutron radiation dose of 25.5 Sv/year and a gamma radiation dose of 3.0 Sv/year. The radiation doses of neutrons and gamma rays were measured using an ionization chamber and a ^{3}He proportional counter, respectively. The actual radiation doses where the high-Tc SQUID monitor is in-

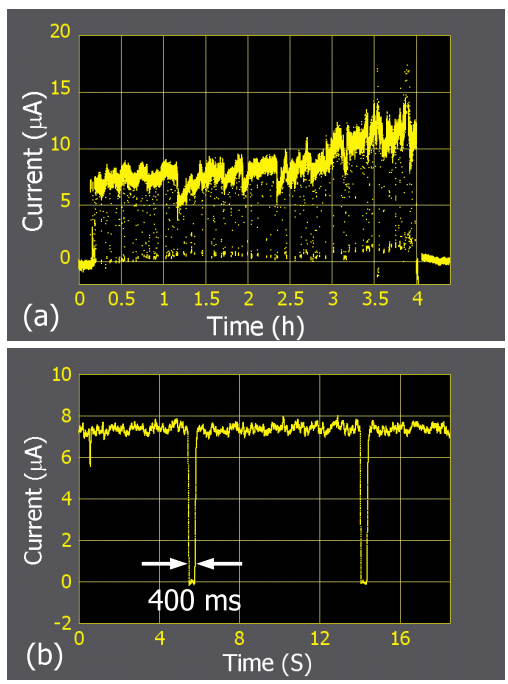

Figure 16: (a) Measurement of 63 MeV/u Ar beam extracted from RRC, which was successfully recorded for approximately 4 h without interrupting beam user experiments. (b) Magnified image of (a) showing dips in current caused by ECR ion source discharge, which recovered within 400 ms.

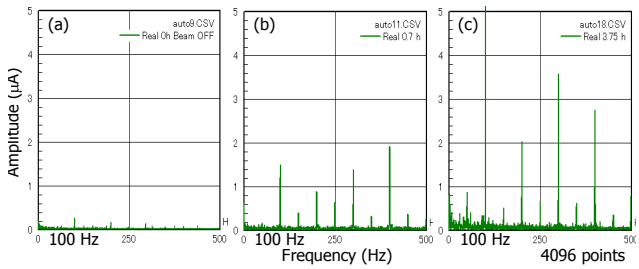

Figure 17: Results analyzed by performing fast Fourier transform (FFT) of measurements shown in Fig. 16(a) at 0 h (beam off) (a), 0.7 h (b) and 3.75 h (c).

stalled are expected to be higher than the above values, because both dosimeters were located 4 m above the high-Tc SQUID monitor. These data gave tentative criteria for judging the risk of radiation damage. After overcoming these difficulties by reinforcing the RF shield and surrounding the FLL circuit with lead and concrete blocks, there were no more problems with the beam current measurement. As a result, a 10 μA $^{40}Ar^{15+}$ beam intensity (63 MeV/u) was successfully measured with 500 nA resolution, as shown in Fig. 15, where a 1 μA beam produced a magnetic flux of $6.5\times10^{-3}\Phi_0$ at the input coil of the high-Tc SQUID.

Furthermore, a prolonged 4 h recording of the Ar beam current extracted from the RRC without interrupting beam user experiments was achieved, as shown in Fig. 16(a). In this recording, several dips in beam intensity due to ECR ion source discharge can be observed at irregular intervals of 10 s to 60 min. Figure 16(b) shows a magnified image of Fig. 16(a), which indicates that the dips in current caused by ECR ion source discharge recovered within 400 ms. The current signals were analyzed by performing a fast Fourier transform (FFT) in the frequency domain, the results of which are shown in Fig. 17. The amplitude of ripples in the modulated beam current increased with the beam current.

All recording and control systems were connected to a PC-based data acquisition system. Through the Ethernet, these systems were linked to a laptop in the main control room located 200 m from the RRC hall. The sampling time for data acquisition was 500 μs, and 100 data points were averaged to improve the S/N ratio.

PRACTICAL USE OF HIGH-T_C SQUID MONITOR FOR RIBF

Upgrade and measurement results

Aiming at its practical use in accelerator operations at the RIBF, we developed a new high-Tc SQUID with a high-permeability core that was installed in the two input coils of the high-Tc SQUID to improve sensitivity [7]. Figure 18 shows a photograph of the new high-Tc SQUID with two holes containing a high-permeability core. The core is composed of 80% Ni and Mo, Re and Fe. The output voltage of the high-Tc SQUID controller as a function of the simulated beam current is plotted in Fig. 19. From these measurement results, the calibration equation is obtained as

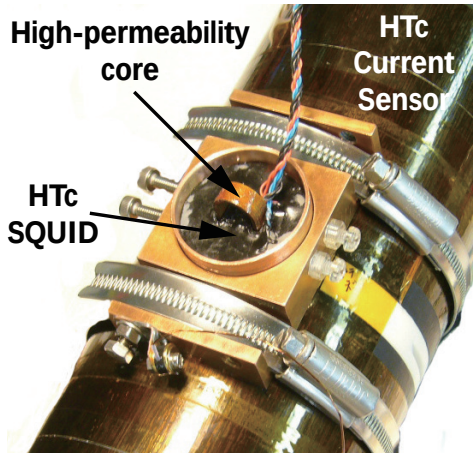

Figure 18: Photograph of new high-Tc SQUID with two holes containing high-permeability core.

$$\begin{aligned} V_s &= S_{co} \times I_b \times G/500 \\ &= 46.60 \times I_b \times G/500, \end{aligned}$$

where S_{co}, I_b, V_s and G are the coupling efficiency (mV/μA), the beam current (μA), the output voltage of the SQUID controller (mV) and the gain, respectively. A test using a simulated beam current indicated a 2-fold improvement in gain, because the coupling efficiency S_{co} of the high-Tc SQUID monitor when it was not equipped with the magnetic core was 22.8 mV/μA. The transfer of the magnetic field produced by the simulated beam current to the SQUID was thus improved. The high-Tc SQUID monitor was upgraded with the new high-Tc SQUID and the mag-

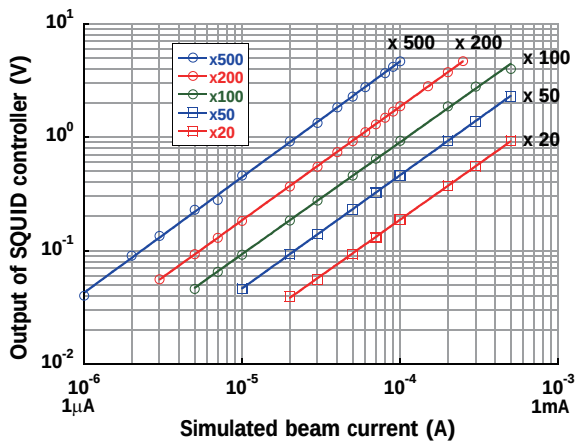

Figure 19: Plot of output voltage of the high-Tc SQUID controller as a function of simulated beam current.

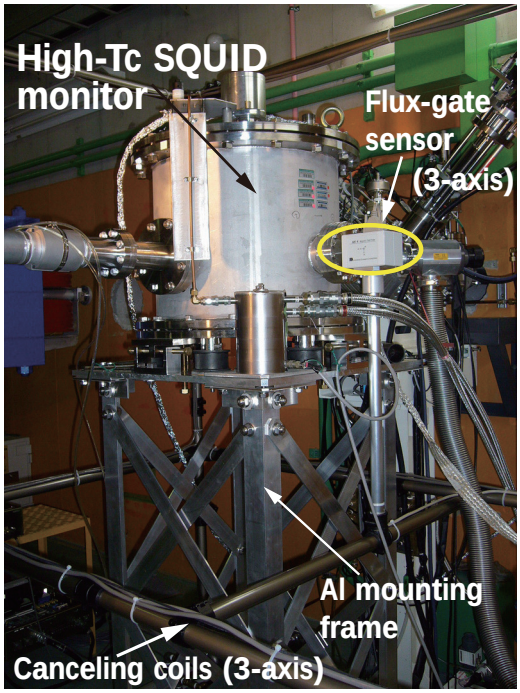

Figure 20: High-Tc SQUID monitor equipped with the Al mounting frame and the noise cancellation system, which was installed in the transport line between the fRC and the IRC (Fig. 1).

netic core, following which the high-Tc SQUID monitor was reassembled. For the purpose of canceling environmental magnetic noise, the previous mounting frame made of iron was replaced with one made of aluminum with a relative permeability of 1. Figure 20 shows the high-Tc

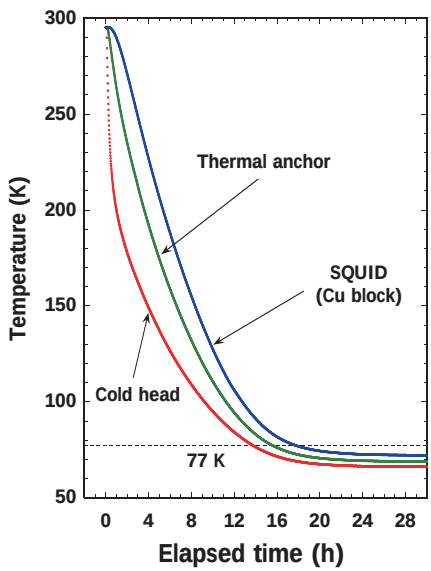

Figure 21: Cooling processes recorded for over 30 h using silicon diode thermometers.

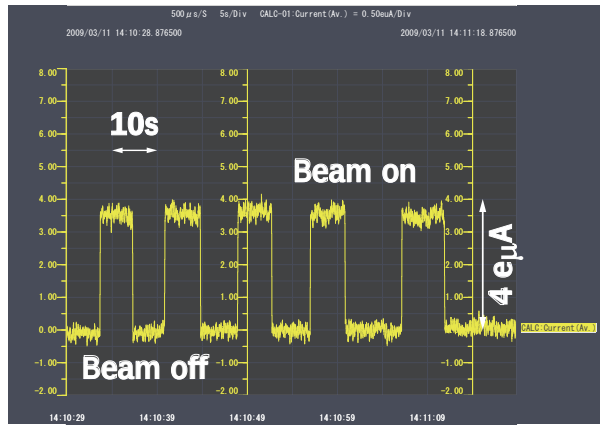

Figure 22: Measurement result for a 3.6 μA $^{132}Xe^{20+}$ (10.8 MeV/u) beam.

SQUID monitor equipped with the Al mounting frame and the noise cancellation system, which was installed in the transport line between the fRC and the IRC (Fig. 1). Figure 21 shows the results of the cooling processes; the temperatures of the cold head, the thermal anchor and the Cu block holding the SQUID were recorded for over 30 h using silicon diode thermometers. The temperature of the high-Tc SQUID was found to reach that of liquid nitrogen (77 K) after 16.5 h. As a result, this year we were able to measure a 3.6 μA $^{132}Xe^{20+}$ (10.8 MeV/u) beam (Fig. 22) and a 1 μA $^{132}Xe^{41+}$ (50.1 MeV/u) beam for use in the accelerator operations at RIBF.

Noise reduction

To obtain a higher measurement resolution, we paid close attention to the reduction of noise. A noise-cut transformer, which is completely isolated from the power circuit and not affected by AC source noise, was introduced to remove normal-mode and common-mode noise, where the noise that flows along one line of the leading wires in one direction and along the other line in the return journey is called normal-mode noise, and the noise that flows along both lines in the outward journey and to earth in the return jouney is called common-mode noise. Furthermore,

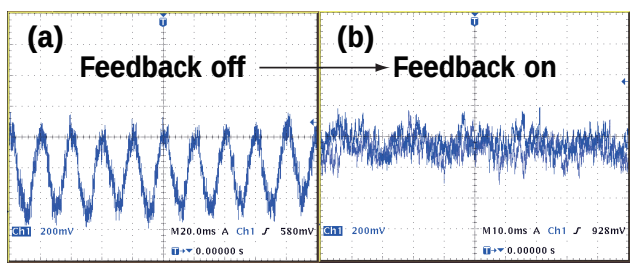

Figure 23: Effect of removing environmental noise by introducing the noise cancellation system.

all instruments were fixed on a large aluminum plate and the grounds of the instruments were connected to the plate. The signal cables were carefully wired to reduce unnecessary loops as much as possible and all AC lines were covered with braided wires.

The design of the noise cancellation system is based on a three-axis Helmholtz cage and feedback control engineering. Three-axis flux-gate sensors are placed near the equipment. A signal is fed through the proprietary controller to a compensation coil, producing precisely calibrated electromagnetic fields. The preliminary result in Figs. 23(a) and (b) shows the effect of the removal of environmental noise by introducing the noise cancellation system.

The data acquisition and control program, currently being written using LabVIEW [21] is almost complete, but some modification is necessary.

The authors are grateful to M. I. Faley of Forschungszentrum Juelich GmbH for valuable discussions on the high-Tc SQUID, A. Ichinose of Central Reserch Institute of Electric Power Industry for fabricating the high-Tc devices and E. Nemoto of JEOL DATUM, Ltd., for cooperation regarding the noise cancellation system.

REFERENCES

[1] Y. Yano, Nucl. Instrum. Methods B **261** (2007) p. 1009.

[2] T. Kubo et al., IEEE Trans. Appl. Supercond. **17** (2003) p. 97.

[3] Y. Yano, Proc. Int. Nuclear Physics Conf. (INPC2007), Tokyo, Japan, June 2007; Proc. 22nd Particle Accelerator Conf. 07 (PAC07), Albuquerque, New Mexico, U.S.A., June 2007.

[4] T. Ohnishi et al., J. Phys. Soc. Jpn. **77** No.8 (2008) p. 083201.

[5] O. Kamigaito et al., Proc. 11th Int. Conf. on Heavy Ion Accelerator Technology (HIAT09), Venice, Italy, June 2009.

[6] T. Watanabe et al., Supercond. Sci. Technol. **17** (2004) p. S450.

[7] T. Watanabe et al., J. Phys. **43** (2006) p. 1215.

[8] T. Watanabe et al., J. Phys. **97** (2008) p. 012248.

[9] I. K. Harvey, Rev. Sci. Instrum., **43** (1972) p. 1626.

[10] K. Grohman, et al., Superconducting quantum interference devices and their applications, Walter de Gruyter & Co. (1977) p. 311.

[11] A. Peters et al., AIP Conf. Proc. **451** (1998) p. 163.

[12] L. Hao et al., IEEE Trans. Appl. Supercond. **11** No.1 (2001) p. 635.

[13] T. Tanabe et al., Nucl. Instrum. Methods Phys. A **427** (1999) p. 455.

[14] Tristan Technologies, http://www.tristantech.com/.

[15] M. I. Faley et al., IEEE Trans. Appl. Supercond. **11** No.1 (2001) p. 1383.

[16] M. I. Faley et al., Supercond. Sci. Technol. **19** (2006) p. S195.

[17] M. I. Faley et al., J. Phys. **43** (2006) p. 1199.

[18] Y. Ishikawa et al., Proc. 4th Int. Symp. on Superconductivity (ISS-4) (1992) p. 1073.

[19] S. Watanabe et al., Proc. 8th European Particle Accelerator Conference (2002) p. 1992.

[20] Vector Fields, http://www.vectorfields.com/.

[21] National Instruments, http://www.ni.com/.